

# On the Spectral Changes of OJ 287: The Lowest X-ray state spectrum– extended at Optical-UV and Hard at X-rays

PANKAJ KUSHWAHA<sup>1,\*</sup>

<sup>1</sup>*Department of Physical Sciences, Indian Institute of Science Education and Research Mohali, Knowledge City, Sector 81, SAS Nagar, Punjab 140306, India*

(Received XXX; Revised YYY; Accepted ZZZ)

## ABSTRACT

Optical-UV synchrotron spectrum has been argued to be the primary driver of the majority of X-ray spectral changes in the BL Lacertae object OJ 287 during its low and intermediate X-ray flux state. Here, we focus on the lowest recorded X-ray flux state of OJ 287 by the Swift facility and report the finding of a power-law optical-UV spectrum with a photon spectrum of  $2.71 \pm 0.03$  continuing into X-rays. Considering this at X-rays, we found a power-law X-ray spectrum of photon spectral index  $1.22 \pm 0.20$  that improves to  $1.29 \pm 0.06$  when considering other observations with similar X-ray spectra. This is the hardest reported X-ray spectrum (0.3–10 keV) and is consistent with the reported Swift-BAT hard X-ray spectrum. We further show that this X-ray spectrum can reproduce most of the flat X-ray spectra when combined with the corresponding optical-UV continuum during the low and intermediate flux states strengthening synchrotron as the primary driver of most of the X-ray spectral changes in the LBL state of the source. Combined with sharp-steepening/cutoff of the optical-UV spectrum during bright phases, the extended-spectrum indicates a comparatively larger emission region and could be the large-scale jet emission. The optical-UV spectrum implies a high-energy power-law particle spectrum of  $\sim 4.4$  while X-ray implies a hard low-energy particle spectrum of  $1.3 - 1.6$  which could be the real or can result from a higher low-energy cut-off in the particle spectrum.

**Keywords:** galaxies: active – BL Lacertae objects: general – quasars: individual – BL Lacertae objects: individual: OJ 287

## 1. INTRODUCTION

OJ 287 is an optically bright BL Lacertae (BLL) type object at a cosmological redshift of  $z=0.306$ , characterized by a non-thermal continuum-dominated optical spectrum with very weak emission line features reported only during its very faint optical brightness states (Sitko & Junkkarinen 1985; Nilsson et al. 2010; Huang et al. 2021). Together with flat spectrum radio quasars (FSRQs), they are referred to as blazars – active galactic nuclei hosting large-scale powerful relativistic jets directed roughly towards the Earth. Blazars are characterized by a highly variable continuum extending across the entire electromagnetic (EM) spectrum from

radio to GeV-TeV gamma-rays that exhibits a broad, bi-model spectral energy distribution (e.g. Abdo et al. 2010; Hayashida et al. 2015; Kushwaha 2022). The temporal continuum variation is primarily erratic and variable at all times from decades and more to all the way to minutes scales accessible within the sensitivities of currently existing facilities (e.g. Goyal et al. 2018).

The low-energy emission component of the bi-model broadband SED that starts at radio and peaks in between near-infrared (NIR) to X-ray energies is widely accepted to be the synchrotron emission from relativistic electrons within the jet due to the non-thermal nature of radio and optical spectrum together with their strong and variable polarization. The high-energy part is debated to be either via inverse Comptonization (IC) – a natural and logical scenario given relativistic electrons and strong photon fields, or hadronic processes or a combination of both (e.g. Gao et al. 2018; Murase & Bartos

Corresponding author: Pankaj Kushwaha  
pankaj.kushwaha@iisermohali.ac.in

\* DST-INSPIRE Faculty Fellow

2019, and references therein). Claims of detection of neutrinos from the direction of these sources support hadronic component and modeling indicates the hadronic component to be sub-dominant at MeV-GeV energies (Gao et al. 2018; Murase & Bartos 2019).

A remarkable property of the bi-modal broadband SED is that the frequency at which the low-energy emission component peaks rarely changes despite the observed strong flux variations, most of which are often accompanied by a change in the continuum spectrum in different observational bands. This stability combined with the physical understanding of the low-energy part of the SED has led to a physical process-based classification of blazars into low- (LSP: LBL+FSRQs), intermediate- (ISP/IBL), and high-synchrotron-peaked blazars (HSP/HBL; Abdo et al. 2010; Fossati et al. 1998).

The inferred dominance of the leptonic component from SED modeling of neutrinos associated blazars e.g. Gao et al. (2018) implies a highly correlated flux variability as well as spectral properties between the EM bands constituting the two humps in the SED. Thus, for simultaneous continuum variation indicating emission from the same region, the spectrum of the low-energy hump is related to that of the high-energy hump. For LBLs/LSPs, to which OJ 287 belongs (e.g. Abdo et al. 2010), this implies a direct connection between the optical-UV (synchrotron) to the MeV-GeV gamma-ray spectrum. The former being purely of synchrotron origin provides a direct tracer of the underlying particle spectrum. Combining this with the simultaneous X-ray spectrum, additionally, allows us to explore the extent of the underlying particle spectrum. This makes the simultaneous optical to X-ray spectrum an excellent observable to probe the high-energy particle spectrum, free from any artifact/complications that could affect the high-energy component e.g. multiple IC fields contributing to the high-energy hump, steepening introduced by the onset of the Klein-Nishina regime as well as extragalactic background light etc. The particle spectrum being the fundamental entity of non-thermal processes has important implications beyond blazar’s high emission, emission region e.g. cosmic rays, astro-particle physics, etc.

Amongst blazars, OJ 287 is one of the best-monitored sources by the transient observing facility: *The Neil Gherels Swift Observatory* because of its frequent activity and peculiar properties (Dey et al. 2018, and references therein), the latter driving most of the coordinated multi-wavelength monitoring (e.g. Seta et al. 2009; Gupta et al. 2017, 2019; Singh et al. 2022; Komossa et al. 2017, 2021). Studies of simulta-

neous<sup>1</sup> optical-to-X-ray spectra have reported a strong anti-correlation between optical-UV and X-ray spectral index (Siejkowski & Wierzcholska 2017). More recently, the source exhibited a very different flux and spectral evolution with drastic spectral changes in all the EM bands (Brien & VERITAS Collaboration 2017; Kushwaha et al. 2018a,b, 2021; Singh et al. 2022; Komossa et al. 2021). The reported spectral phases are unique and OJ 287 is the very first blazar to exhibit spectra that are representative of the entire blazar class (e.g. Kushwaha 2022; Singh et al. 2022). Theoretical scenarios based modeling of the simultaneous optical to X-ray SED reports both – a continuation of the optical-UV spectrum (synchrotron) into X-ray bands, making the X-ray spectrum relatively flatter/softer (Singh et al. 2022; Pal et al. 2020; Isobe et al. 2001) as well as a sharp steepening of the optical-UV spectrum at (far) UV energies (Singh et al. 2022; Seta et al. 2009).

In the current work, we focus on a detailed spectral investigation of the simultaneous optical to X-ray spectrum of the observed lowest X-ray flux state of OJ 287 by the *Swift* observatory. The work is organized as follows. In the next section (§2), we present the details of the data and reduction procedure. Section §3 presents the analysis and results reporting an optical-UV synchrotron spectrum extending to X-ray energies and the hardest X-ray spectrum of the source during the lowest X-ray flux state. Section §4 presents the implications of this on particle acceleration scenarios emission mechanisms with a summary in §5.

## 2. DATA REDUCTION

The *Neil Gherels Swift* Observatory (Gehrels et al. 2004) is a space-based facility with three primary payloads – X-Ray Telescope (XRT; 0.3 – 10 keV), Ultra-violet Optical Telescope (UVOT), and the Burst Alert Telescope (BAT; 15–150 keV) capable of simultaneously observing optical to hard X-ray band over a wide range of source brightness state. In this work, we used all the pointed XRT and UVOT data of OJ 287<sup>2</sup> till December 2022 (MJD: 53510 – 59940) to perform the spectral study. The dense *Swift* follow-up since mid-2015 has been carried out by Komossa et al. (2017, 2021)<sup>3</sup>.

**UVOT:** The UVOT data of the source was reduced following the methodology adopted in Kushwaha et al.

<sup>1</sup> not strictly, exposure/data-extraction vary significantly in different bands– order of a few minutes at optical while sub-hour to hour at X-rays.

<sup>2</sup> source too faint for spectral/flux studies at BAT energies on ID-wise timescale e.g. Langejahn et al. (2020).

<sup>3</sup> the project is now called “MOMO” by the PIs

(2021). We used a  $5''$  circular region for the source and an annular source-free region of inner and outer radii of  $25''$  and  $45''$  respectively for the background, both centred on the source location. We then executed the *HEASOFT* (v6.30.1) tasks *uvotsum* and *uvotsource* to extract the flux density in each filter. The extracted flux densities were subsequently corrected for reddening using an  $E(B-V) = 0.0241$  with the extinction law of Cardelli et al. (1989).

**XRT:** For the X-ray spectral study, we directly used the scientific grade spectra and respective ancillary files provided by the UKSSDC<sup>4</sup>. The underlying pipeline corrects for pile-up in both photon counting (PC) and window timing (WT) mode data following the procedure detailed in Evans et al. (2009) and subsequent ongoing updates. For OJ 287, none of the WT mode data requires pile-up treatment (rate  $\ll 100$  c/s) while PC mode data having count rate  $\gtrsim 0.5$  c/s were marked for pile-up correction.

To find the best description of the X-ray spectrum, we followed the approach adopted in Kushwaha et al. (2018b, 2021) using *F-test* statistics to choose the best-fit description between the absorption (tbabs) modified power-law (PL;  $dN/dE \sim E^{-\Gamma}$ ) and log-parabola (LP;  $dN/dE \sim E^{-\alpha - \beta \log(E)}$ ) models. We used a *F-test* value of 0.01 below which LP is preferred and vice-versa. We binned each source spectral file with a minimum of one count per bin and performed the model fitting (0.3–10 keV) using the *Cash – statistics* with background (W Statistic in XSPEC). During the model fitting, we kept all the parameters free initially but froze the nH value to the Galactic column density of  $2.4 \times 10^{20} \text{ cm}^{-2}$  (HI4PI Collaboration et al. 2016) in the direction of the source, whenever the fit value was equal or below it. Finally, for spectral study, we corrected all the extracted X-ray SEDs for nH absorption.

### 3. SED ANALYSIS AND RESULTS

The optical to X-ray light curve and spectral behavior extracted from the *Swift* facility are shown in Figure 1. The UVOT spectral index is extracted assuming a PL model. The source has undergone a strong flux variation of  $> 100$  in X-ray and  $\gtrsim 15$  in UVOT bands between the minimum and maximum during this period. An interesting behavior is the concurrent low-flux state in both optical-UV and X-ray, marked in the cyan-colored band in Fig. 1 (MJD  $\sim 54160 - 54180$ ) with the lowest X-ray flux within the cadence, statistics, and instrument sensitivity. Later, though optical-UV has even gone be-

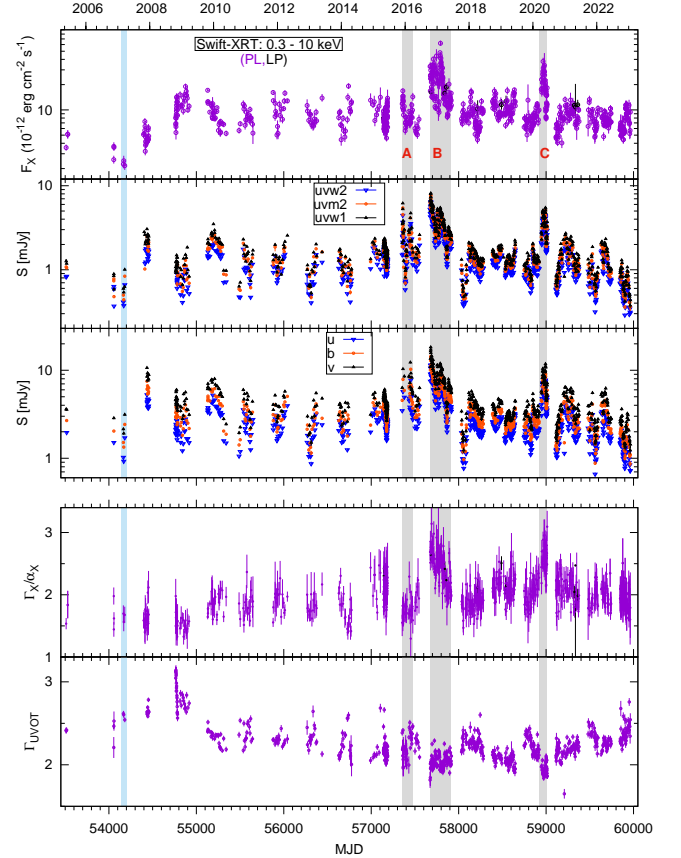


**Figure 1.** Optical to X-ray light curve of OJ 287 from the *Swift* facility observation between 2005 to 2022 (ref §2). The spectral index from the best fit PL/LP model for X-ray and the PL model of optical-UV is shown in the bottom panels. The cyan band is the focus of this work while the dark-shaded regions mark the duration with very different spectral features across the EM bands e.g. A: Kushwaha et al. (2018a); B: Kushwaha et al. (2018b); C and in-between B-C: Kushwaha et al. (2021).

low this level, the X-ray has not. Another point to be noted is fewer X-ray points with LP model in Figure 1 compared to our previous work Kushwaha (2022). The difference is due to the *F-test* probability value used: 0.01 here compared to 0.05 in Kushwaha (2022). We chose a tighter value because the low-flux states –the focus of our study, favor the PL<sup>5</sup> model.

Since our focus is the lowest X-ray flux state and synchrotron is known to affect the X-ray spectrum (Singh et al. 2022; Pal et al. 2020; Isobe et al. 2001), we ordered the IDs first by X-ray flux (increasing) and then filtered all the IDs with best-fit X-ray flux within  $3\sigma$  of the lowest X-ray flux (resulting in 4 IDs). Among these,

<sup>4</sup> [https://www.swift.ac.uk/user\\_objects/](https://www.swift.ac.uk/user_objects/)

<sup>5</sup> relaxing *F-test* value will have no effect on the outcome. It primarily affects the gray shaded part (A, B, C) of Figure 1

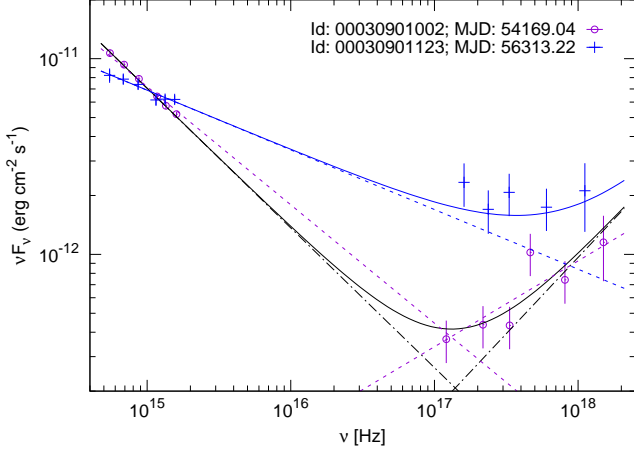


**Figure 2.** The optical to X-ray SED corresponds to the lowest identified X-ray state in purple along with an intermediate state showing a relatively flat X-ray spectrum. The purple dashed lines are the best-fit PL model to optical-UV and X-ray (PL :  $\Gamma_X = 1.5 \pm 0.1$ ) separately while the black dot-dashed lines are the best-fit from the joint fit of the optical to X-ray with the solid black curve representing the overall spectrum. The flat X-ray spectra of the intermediate state (blue curve) can be simply reproduced by adding the hard X-ray spectrum from the joint-fit to the corresponding optical-UV synchrotron spectrum.

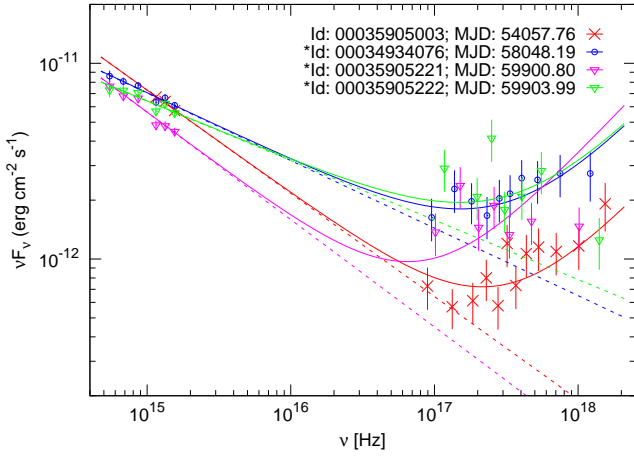


**Figure 3.** A subset of X-ray spectra, representative of the observed X-ray spectra during low and intermediate X-ray flux states, demonstrates that the flat X-ray spectrum can be simply reproduced by adding the inferred hard X-ray component to the respective optical-UV PL spectrum shown by dashed curves. The ones marked with '\*' however require variation in normalization (up to a factor of 3 here) of the inferred harder X-ray spectrum and in a few cases, a different spectrum.

we then looked for the ID with the lowest flux in UVOT bands (ID: 00030901002). The corresponding optical to X-ray SEDs for this is shown in Figure 2.

As optical-UV is synchrotron emission, to get the spectral index, we first fitted a PL model to the UVOT SED using  $\chi^2$  statistic in XSPEC. We then extrapolated the best-fit optical-UV spectrum and examined it vis-a-vis the corresponding X-ray spectrum. We found that the UVOT PL fit ( $\Gamma_{\text{UVOT}} = 2.71 \pm 0.03$ ) extends well into X-ray. Thus, to get the uncontaminated X-ray spectral parameter, we jointly modeled the optical to X-ray spectrum with a two-PL model (redden\*powerlaw + tbabs\*powerlaw), for the reddening modified optical-UV PL model contribution to X-ray energies. We found a harder X-ray photon spectral index of  $\Gamma_X = 1.22 \pm 0.20$  compared to  $\Gamma_X \sim 1.5$  when fitting X-ray alone.

To further improve the constraint, we jointly modeled all the observation IDs (total 7 IDs) having similar X-ray spectral indices (hard;  $\Gamma_X : 1.2 - 1.3$ ). This resulted in an improved constraint of  $\Gamma_X = 1.29 \pm 0.06$  using  $\chi^2$ -statistic for UVOT and *Cash - statistic* at X-rays. We re-checked the result using only  $\chi^2$ -statistic at both optical-UV and X-ray with X-ray binned to a minimum of 20 counts per bin. We got a consistent result (within  $1\sigma$ ;  $\Gamma_X = 1.16 \pm 0.08$ ;  $\chi^2/\text{dof}^6 = 67.4/61$ ) but this lacks the lowest X-ray flux state due to insufficient counts. The best-fit model from the lowest X-ray flux state along with data is shown in Figure 2. This is the hardest-ever reported X-ray spectrum (0.3 - 10 keV) for OJ 287 to the best of our knowledge.

We then explored other low and intermediate X-ray flux states, most of which have a relatively flatter X-ray spectrum ( $\Gamma \sim 1.7 - 2.1$ ) and found that this inferred hard X-ray spectrum without or with variation of normalization along with the respective optical-UV spectrum can naturally explain a majority of the observed flat X-ray spectrum of the LBL phase of the source. A subset of such IDs, representative of the different X-ray spectra exhibited by the source are shown in Figures 2 and 3. We also found that a few are indeed different spectrally. These and the observation-IDs requiring change of normalization of the inferred hard X-ray spectrum are marked with '\*' in Figure 3.

#### 4. DISCUSSION

We found an extended optical-UV synchrotron spectrum ( $\Gamma_{\text{UVOT}} = 2.71 \pm 0.03$ ), continuing into X-rays during a period with concurrent dip in optical-UV and X-ray flux (MJD: 54160 - 54180; cyan band in Fig. 1), corresponding to the lowest reported X-ray flux within the *Swift* cadence. Accounting for this contribution at X-rays, we found a hard X-ray spectrum with photon spectral index  $\Gamma_X \sim 1.15 - 1.3$  (0.3-10 keV; ref Fig. 2),

<sup>6</sup> degree of freedom



the hardest ever reported from the study of simultaneous optical to X-ray spectrum of OJ 287. This is in contrast to the bright/active state optical X-ray SEDs of the source where the X-ray spectrum generally implies a cutoff or sharp steepening of the optical-UV synchrotron spectra in the (far) UV region (e.g. Singh et al. 2022; Seta et al. 2009). This X-ray spectrum is consistent with the spectrum reported in the hard X-ray band from *Swift*-BAT measurement (50-300 keV; Langejahn et al. 2020). We further found that a majority of the flat X-ray spectra during the low and intermediate X-ray flux states can be naturally explained by simply adding the inferred hard X-ray spectrum with the respective optical-UV spectrum either originally or with a variation of the normalization (ref Figs. 2 and 3). A few cases, however, indeed have different spectrum (refer to Fig. 3).

Blazar optical continuum is well-understood to be synchrotron and thus, the observed spectrum directly traces the underlying particle spectrum. The same holds for the IC spectrum i.e. X-ray, if its away from the peak and IC happens in the Thomson regime. For a power-law particle distribution of spectral index  $p$  ( $N(E) \sim E^{-p}$ ), the observed radiation energy spectrum is  $f \sim E_{\text{ph}}^{-(p-1)/2}$ . OJ 287 being an LBL source, the X-ray is a good tracer of the low-energy part while the optical-UV directly traces the high-energy part of the broken power-law particle distribution required for broadband SED modeling (e.g. Singh et al. 2022). The reported optical to X-ray spectrum corresponding to the lowest X-ray flux thus implies a hard low-energy particle spectrum of  $1.3 - 1.6$  and a high-energy spectrum of  $\sim 4.4$ .

For blazar's synchrotron spectrum, the observed frequency is related to the rest frame via  $\nu_{\text{obs}} = \delta/(1+z)\gamma^2\nu_L$  where  $\nu_L$  is the Larmor frequency,  $\gamma$  is the electron Lorentz factor, and  $\delta$  is the bulk Doppler factor. Further,  $\nu_L = eB/2\pi m_e c$ , depends solely on the magnetic field,  $B$ . Thus for a given  $B$  and  $\delta$ , the extent of the spectrum depends on the Lorentz factor (energies) of the particles. Since X-ray lies at the tail of the high-energy synchrotron spectrum, the combined optical to X-ray spectrum thus provides a potential direct tracer of the extent of the high-energy particle spectrum. The finding of an extended optical-UV synchrotron spectrum reported here clearly indicates a much extended high-energy particle spectrum compared to the bright X-ray phases of the source. On the other hand, the natural explanation of most of the flat X-ray spectra associated with the low and intermediate X-ray flux states of the LBL/LSP state of the source by adding the high-energy synchrotron tail to the lowest hard X-ray spectrum further strengthens previous claims/finding that most of

the X-ray spectral changes are due to optical-UV synchrotron spectrum (Singh et al. 2022).

The relativistic particle spectrum has two main ingredients – the spectral index and the extent (energy-limits) of the spectrum. The spectral index is related to the particle acceleration processes and the extent of the spectrum is related to the size of the acceleration region – the Hilas energy criteria (Hillas 1984). The reported extended high-energy spectrum implies a comparatively larger acceleration/emission region compared to the flaring states that in general indicate a steepening or cutoff. The inference is also consistent with short variability timescales, indicating a compact emission region during flares. Indirectly the larger acceleration/emission region could possibly be the large-scale jet emission. Since the reported hard X-ray is sum of synchrotron tail and IC – mostly of the low-energy part of particle distribution, a harder spectrum at X-ray may not be a direct reflection of harder particle spectrum but can also result from a higher-lower-energy cutoff of the underlying particle spectrum (Inoue & Takahara 1996) – consistent with a larger acceleration/emission region argued above. But if its actual then the lower-limit of the hard particle spectrum indicates magnetic reconnection as the most likely driver (e.g. Guo et al. 2014) while the upper-limit appears consistent with the shock scenario (Malkov & Drury 2001).

Though OJ 287 has been studied extensively at all wavelengths, and especially at optical and X-rays, most of the studies focusing on the latter have separately explored optical-UV and X-rays (e.g. Siejkowski & Wiercholska 2017; Kushwaha et al. 2021; Komossa et al. 2022, and references therein) or the X-ray flux have been comparatively higher (e.g. Singh et al. 2022; Seta et al. 2009). Given the blazar broadband emission, a consideration of all likely processes is a must to gain further insight into the source behavior and thus, the jet physics, extra/hidden emission components, etc. A detailed outcomes of this systematic analysis will be presented in the accompanying paper (Kushwaha 2023, in preparation).

## 5. SUMMARY AND CONCLUSIONS

We explored the simultaneous optical to X-ray observations (spectra) of the BL Lacertae object OJ 287 by the *Neils Geherel's Swift Observatory* to date with a focus on the lowest X-ray state and found a power-law optical-UV synchrotron continuum of photon spectral index  $\Gamma_{\text{UVOT}} = 2.71 \pm 0.03$  that extends to X-ray energies. Modeling the corresponding X-ray spectrum accounting synchrotron component contribution, we found a hard 0.3-10 keV X-ray spectrum with  $\Gamma_X \sim$

1.15 – 1.3. This is harder than the reported hardest spectrum ( $\Gamma_X \sim 1.5$ ) considering only the X-ray data and is consistent with the hard X-ray spectrum reported from the *Swift*-BAT data (20–100 keV). The optical-UV directly traces the underlying high-energy particle spectrum with a PL spectrum of  $\sim 4.4$  while X-ray implies a harder PL spectrum of 1.3 – 1.6. The harder spectrum in the latter case may not be real and could result from a comparatively higher lower-energy-cutoff in the particle spectrum.

The reported hard X-ray can naturally explain most of the observed flat X-ray spectra when combined with the corresponding optical-UV spectrum. The finding further strengthens previous claim that most of the flat X-ray spectra of the source in the LBL/LSP spectral phase of the source are due to the optical-UV synchrotron spectrum extending to X-ray energies.

The extended optical-UV spectrum implies an extended high-energy particle spectrum, and thus, a rela-

tively large acceleration/emission region size per the Hillas criteria and is consistent also with the indication of a comparatively higher lower-energy-cutoff in the particle spectrum implied from the hard X-ray spectrum. The larger size suggests the inferred low-emission component could possibly be associated with the large-scale jet.

## ACKNOWLEDGMENTS

The author thank the anonymous referees for valuable inputs and suggestions. The author acknowledges financial support from the Department of Science and Technology (DST), Government of India, through the DST-INSPIRE faculty grant (DST/INSPIRE/04/2020/002586). This work made use of data supplied by the UK Swift Science Data Centre at the University of Leicester.

*Facilities:* Swift.

*Software:* Gnuplot (version: 5.2; <http://www.gnuplot.info/>), SHERPA, HEASOFT

## REFERENCES

- Abdo, A. A., Ackermann, M., Agudo, I., et al. 2010, *ApJ*, 716, 30, doi: [10.1088/0004-637X/716/1/30](https://doi.org/10.1088/0004-637X/716/1/30)
- Brien, S. O., & VERITAS Collaboration. 2017, in International Cosmic Ray Conference, Vol. 301, 35th International Cosmic Ray Conference (ICRC2017), 650, doi: [10.22323/1.301.0650](https://doi.org/10.22323/1.301.0650)
- Cardelli, J. A., Clayton, G. C., & Mathis, J. S. 1989, *ApJ*, 345, 245, doi: [10.1086/167900](https://doi.org/10.1086/167900)
- Dey, L., Valtonen, M. J., Gopakumar, A., et al. 2018, *ApJ*, 866, 11, doi: [10.3847/1538-4357/aadd95](https://doi.org/10.3847/1538-4357/aadd95)
- Evans, P. A., Beardmore, A. P., Page, K. L., et al. 2009, *MNRAS*, 397, 1177, doi: [10.1111/j.1365-2966.2009.14913.x](https://doi.org/10.1111/j.1365-2966.2009.14913.x)
- Fossati, G., Maraschi, L., Celotti, A., Comastri, A., & Ghisellini, G. 1998, *MNRAS*, 299, 433, doi: [10.1046/j.1365-8711.1998.01828.x](https://doi.org/10.1046/j.1365-8711.1998.01828.x)
- Gao, S., Fedynitch, A., Winter, W., & Pohl, M. 2018, *Nature Astronomy*, 154, doi: [10.1038/s41550-018-0610-1](https://doi.org/10.1038/s41550-018-0610-1)
- Gehrels, N., Chincarini, G., Giommi, P., et al. 2004, *ApJ*, 611, 1005, doi: [10.1086/422091](https://doi.org/10.1086/422091)
- Goyal, A., Stawarz, L., Zola, S., et al. 2018, *ApJ*, 863, 175, doi: [10.3847/1538-4357/aad2de](https://doi.org/10.3847/1538-4357/aad2de)
- Guo, F., Li, H., Daughton, W., & Liu, Y.-H. 2014, *PhRvL*, 113, 155005, doi: [10.1103/PhysRevLett.113.155005](https://doi.org/10.1103/PhysRevLett.113.155005)
- Gupta, A. C., Agarwal, A., Mishra, A., et al. 2017, *MNRAS*, 465, 4423, doi: [10.1093/mnras/stw3045](https://doi.org/10.1093/mnras/stw3045)
- Gupta, A. C., Gaur, H., Wiita, P. J., et al. 2019, *AJ*, 157, 95, doi: [10.3847/1538-3881/aafe7d](https://doi.org/10.3847/1538-3881/aafe7d)
- Hayashida, M., Nalewajko, K., Madejski, G. M., et al. 2015, *ApJ*, 807, 79, doi: [10.1088/0004-637X/807/1/79](https://doi.org/10.1088/0004-637X/807/1/79)
- HI4PI Collaboration, Ben Bekhti, N., Flöer, L., et al. 2016, *A&A*, 594, A116, doi: [10.1051/0004-6361/201629178](https://doi.org/10.1051/0004-6361/201629178)
- Hillas, A. M. 1984, *ARA&A*, 22, 425, doi: [10.1146/annurev.aa.22.090184.002233](https://doi.org/10.1146/annurev.aa.22.090184.002233)
- Huang, S., Hu, S., Yin, H., et al. 2021, *ApJ*, 920, 12, doi: [10.3847/1538-4357/ac0eff](https://doi.org/10.3847/1538-4357/ac0eff)
- Inoue, S., & Takahara, F. 1996, *ApJ*, 463, 555, doi: [10.1086/177270](https://doi.org/10.1086/177270)
- Isobe, N., Tashiro, M., Sugihro, M., & Makishima, K. 2001, *PASJ*, 53, 79, doi: [10.1093/pasj/53.1.79](https://doi.org/10.1093/pasj/53.1.79)
- Komossa, S., Grupe, D., Schartel, N., et al. 2017, in *New Frontiers in Black Hole Astrophysics*, ed. A. Gomboc, Vol. 324, 168–171, doi: [10.1017/S1743921317001648](https://doi.org/10.1017/S1743921317001648)
- Komossa, S., Grupe, D., Parker, M. L., et al. 2021, *MNRAS*, 504, 5575, doi: [10.1093/mnras/stab1223](https://doi.org/10.1093/mnras/stab1223)
- Komossa, S., Grupe, D., Kraus, A., et al. 2022, *MNRAS*, 513, 3165, doi: [10.1093/mnras/stac792](https://doi.org/10.1093/mnras/stac792)
- Kushwaha, P. 2022, *Journal of Astrophysics and Astronomy*, 43, 79, doi: [10.1007/s12036-022-09872-1](https://doi.org/10.1007/s12036-022-09872-1)
- . 2023, in prep
- Kushwaha, P., Pal, M., Kalita, N., et al. 2021, *ApJ*, 921, 18, doi: [10.3847/1538-4357/ac19b8](https://doi.org/10.3847/1538-4357/ac19b8)
- Kushwaha, P., Gupta, A. C., Wiita, P. J., et al. 2018a, *MNRAS*, 473, 1145, doi: [10.1093/mnras/stx2394](https://doi.org/10.1093/mnras/stx2394)
- . 2018b, *MNRAS*, 479, 1672, doi: [10.1093/mnras/sty1499](https://doi.org/10.1093/mnras/sty1499)

- Langejahn, M., Kadler, M., Wilms, J., et al. 2020, A&A, 637, A55, doi: [10.1051/0004-6361/202037469](https://doi.org/10.1051/0004-6361/202037469)
- Malkov, M. A., & Drury, L. O. 2001, Reports on Progress in Physics, 64, 429, doi: [10.1088/0034-4885/64/4/201](https://doi.org/10.1088/0034-4885/64/4/201)
- Murase, K., & Bartos, I. 2019, Annual Review of Nuclear and Particle Science, 69, 477, doi: [10.1146/annurev-nucl-101918-023510](https://doi.org/10.1146/annurev-nucl-101918-023510)
- Nilsson, K., Takalo, L. O., Lehto, H. J., & Sillanpää, A. 2010, A&A, 516, A60, doi: [10.1051/0004-6361/201014198](https://doi.org/10.1051/0004-6361/201014198)
- Pal, M., Kushwaha, P., Dewangan, G. C., & Pawar, P. K. 2020, ApJ, 890, 47, doi: [10.3847/1538-4357/ab65ee](https://doi.org/10.3847/1538-4357/ab65ee)
- Seta, H., Isobe, N., Tashiro, M. S., et al. 2009, Publications of the Astronomical Society of Japan, 61, 1011, doi: [10.1093/pasj/61.5.1011](https://doi.org/10.1093/pasj/61.5.1011)
- Siejkowski, H., & Wiercholska, A. 2017, MNRAS, 468, 426, doi: [10.1093/mnras/stx495](https://doi.org/10.1093/mnras/stx495)
- Singh, K. P., Kushwaha, P., Sinha, A., et al. 2022, MNRAS, 509, 2696, doi: [10.1093/mnras/stab3161](https://doi.org/10.1093/mnras/stab3161)
- Sitko, M. L., & Junkkarinen, V. T. 1985, PASP, 97, 1158, doi: [10.1086/131679](https://doi.org/10.1086/131679)